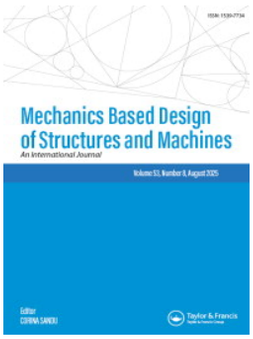

Taylor & Francis
Taylor & Francis Group

Mechanics Based Design of Structures and Machines

An International Journal

ISSN: 1539-7734 (Print) 1539-7742 (Online) Journal homepage: www.tandfonline.com/journals/lmbd20

High control performance of tuned two-mass damper using grounded inerters for vibration control of civil structures

Ngoc-An Tran, Van-Binh Bui & Quoc-Huong Cao

To cite this article: Ngoc-An Tran, Van-Binh Bui & Quoc-Huong Cao (03 Jun 2025): High control performance of tuned two-mass damper using grounded inerters for vibration control of civil structures, Mechanics Based Design of Structures and Machines, DOI: 10.1080/15397734.2025.2509255

To link to this article: https://doi.org/10.1080/15397734.2025.2509255

Published online: 03 Jun 2025.

MECHANICS BASED DESIGN OF STRUCTURES AND MACHINES
https://doi.org/10.1080/15397734.2025.2509255

High control performance of tuned two-mass damper using grounded inerters for vibration control of civil structures

Ngoc-An Tran[a], Van-Binh Bui[b], and Quoc-Huong Cao[c]

[a]Faculty of Civil Engineering, Vietnam Maritime University, Haiphong, Vietnam; [b]Faculty of Mechanical-Automotive and Civil Engineering, Electric Power University, Hanoi, Vietnam; [c]Faculty of Engineering and Information Technology, School of Mechanical and Mechatronic Engineering, University of Technology Sydney, Sydney, Australia

ABSTRACT

A Tuned Two-Mass Damper (TTMD), which consists of two undamped tuned mass dampers connected by a dashpot, has been demonstrated to be more effective than a traditional TMD. To improve the effectiveness and robustness of TTMD, an innovative type of TTMD used for structural vibration control is developed in this work. This innovative version consists of a TTMD connected to the ground by one or two inerters (TTMDGI). In this study, the three inerter-based configurations of TTMD are proposed. After developing three analytical models of the system with one of the proposed TTMDGI configurations, the optimal parameters of each TTMDGI configuration for various values of inertance are determined. From that, the performance and robustness of each TTMDGI configuration are calculated and compared to the inerter-based tuned mass damper. Additionally, the effects of the weight and inertance of each TTMDGI configuration on the structural response are investigated. This research indicates that the inerter-based configurations of TTMD are much more effective and robust than the TTMD. Furthermore, the performance of each optimal TTMDGI configuration significantly exceeds that of the optimal inerter-based Tuned Mass Damper (TMDI) with the same mass and inertance ratio. The effectiveness improvement is from 30.2 to 36.3% in the dynamic magnification factor of the structural response compared to TMDI as the inertance ratio rises from 1 to 5%. This significantly reduces the device's weight added to the structure if using a TTMDGI configuration instead of a TMDI.

ARTICLE HISTORY
Received 10 January 2025
Accepted 12 May 2025

KEYWORDS
Vibration control; inerter-based tuned two-mass damper; tuned two-mass damper; inerter-based tuned mass damper; passive vibration absorber; multi-objective optimization

1. Introduction

Reducing the vibrational response of structures is a very important objective, especially in the field of civil engineering. Natural hazards like earthquakes and strong storms may induce vibrations of civil structures with large amplitudes. This leads to severe consequences, including significant harm to structures and occupants (Balendra, Wang, and Cheong 1995; Cao 2021; Shah and Usman 2022). Various solutions have been studied and implemented to mitigate the impact of structural vibrations, among which the use of vibration absorbers, such as Tuned Mass

CONTACT Quoc-Huong Cao huong.q.cao@student.uts.edu.au Faculty of Engineering and Information Technology, School of Mechanical and Mechatronic Engineering, University of Technology Sydney, Sydney, New South Wales, Australia
Communicated by Xiaoying Zhuang.

Damper (TMD) or Tuned Liquid Column Damper (TLCD), has emerged as one of the most effective and widely utilized technologies in civil engineering (Bui, Tran, and Cao 2023; Cao 2021; Cao and Tran 2023; Momtaz, Abdollahian, and Farshidianfar 2017). Unlike active, semi-active, and hybrid systems that need control algorithms and required energy sources for their operation, passive control devices do not require a control algorithm and external energy source. Thanks to their simplicity and independence from external energy, passive vibration absorbers are more widely used than active, semi-active, and hybrid control systems in civil structures (Cao 2021; Ma, Bi, and Hao 2021; Tran et al. 2025).

On the other hand, the first concept of inerter was proposed by Smith (2002). Since then, different types of inerter have been developed. To further improve the vibration control performance of a traditional TMD or TLCD, researchers have integrated inerters into TMDs or TLCDs (Giaralis and Petrini 2017; Marian and Giaralis 2014; Pietrosanti, De Angelis, and Basili 2020; Pietrosanti, De Angelis, and Giaralis 2020). For example, based on the "mass amplification effect" from the inerter, Marian and Giaralis proposed an innovative configuration of TMD to suppress the oscillatory motion of stochastically excited mechanical systems (Marian and Giaralis 2014). Giaralis and Petrini employed a conventional TMD coupled with an inerter (referred to as a TMDI) to reduce wind-induced oscillations of high-rise buildings, in which various TMDI topologies were also proposed (Giaralis and Petrini 2017). Madhamshetty and Manimala conducted analytical and experimental studies on the low-rate characterization of a mechanical inerter, in which improved analytical models that consider the effects of component inertias and sizing for both the ball-screw and rack-and-pinion versions of the inerter were investigated (Madhamshetty and Manimala 2018). For dynamic vibration absorbers (DVAs), Kendo-Nouja et al. developed the DVA with a grounded inerter that efficiently mitigates dynamic responses of structures under different types of excitations (Kendo-Nouja et al. 2024). Baduidana and Kenfack-Jiotsa introduced a three-element DVA with grounded stiffness and an attached inerter, designed for suppressing vibrations in undamped SDOF structures (Baduidana and Kenfack-Jiotsa 2024). Meanwhile, Pandey and Mishra developed the compliant liquid column damper with an inerter (TLCDI) to suppress vibrational responses for both single-degree-of-freedom (SDOF) and multi-degree-of-freedom (MDOF) structures under the recorded motions (Pandey and Mishra 2021). Wang et al. successfully used a TLCDI to significantly mitigate the seismic response of SDOF structures (Wang et al. 2020), while Masnata et al. proposed a nontraditional configuration of TLCDI for base-isolated structures (Masnata et al. 2023). The notable findings from the above works show that inerter-based vibration absorbers outperform traditional ones, contributing an outstanding solution for controlling vibrations in different civil structures.

In 2024, Cao et al. developed an innovative model of Tuned Mass Damper (TMD), referred to as the Tuned Two-Mass Damper (TTMD) (Cao, Tran, and Nguyen 2024). This device is a passive vibration absorber designed to reduce structural responses. The TTMD consists of two undamped tuned mass dampers connected by a dashpot. Their research showed that the TTMD outperforms a traditional TMD with the equivalent weight as TTMD. Building on their foundational research and to further improve the effectiveness and robustness of a TTMD, three different configurations of the TTMD with inerters for structural vibration control are proposed in this study. In these innovative configurations, the TTMDs are connected to the ground using either one or two linear inerters (denoted as TTMDGI).

The paper is organized as follows. After the introduction, Section 2 presents three analytical models of TTMDGI integrated into an SDOF structure under an external force. Section 3 is to determine the optimal parameters of each TTMDGI configuration using a potential optimization algorithm. Based on the optimal parameters found in Section 3, the vibration control performance and robustness of each TTMDGI configuration are predicted and compared with an

optimum Inerter-Based Tuned Mass Damper (TMDI) in Section 4. Finally, noticeable conclusions from this work are stated in Section 5.

2. Theoretical analysis and modeling

In this section, the concept and working principle of inerters are mentioned. Next, three different configurations of the TTMD coupled with inerters for vibration control of an SDOF structure are presented.

2.1. Inerters and their working principles

Many different types of inerter include the ball-screw, rack-and-pinion, hydraulic, helical fluid, electromagnetic, and living-hinge types (Konar and Ghosh 2024; Liu et al. 2018; Ma, Bi, and Hao 2021). The rack-pinion type, ball-screw type, and hydraulic type inerters are most common based on the mechanism of inertial amplification (Konar and Ghosh 2024; Ma, Bi, and Hao 2021; Pandey and Mishra 2021). A schematic of a rack-pinion type inerter is shown in Fig. 1(a). This rack-pinion type inerter consists of an assembly that includes two terminals, one rack, one gear, two pinions, and a flywheel. One terminal is the end of the rack, while the other of the rack is connected to the flywheel. The translational motion from the rack terminal is amplified by the pinion-gear assembly and transmitted through the flywheel (Wang et al. 2020).

A ball-screw type inerter, as depicted in Fig. 1(b), comprises four main components: a flywheel, a lead screw, a flywheel chamber, and a screw stroke chamber. The flywheel is fixed at one end of the lead screw within the flywheel chamber, while the other end of the lead screw is extended into the screw stroke chamber. A screw nut is positioned on the lead screw to facilitate its motion and enhance the amplification of inertial forces (Shen et al. 2016). The hydraulic type inerter consists of a fluid chamber with a piston and an alternative parallel flow path for the fluid, as illustrated in Fig. 1(c). When there is relative movement between the two terminals, the fluid flows through the alternate tube, creating a gap between the piston and the fluid chamber. This gap generates pressure differences, which amplify inertia. Additionally, the compressibility of the fluid contributes to this amplification (Chillemi et al. 2023; Liu et al. 2018).

According to Smith (2002, 2020), Fig. 1(d) shows a schematic of an ideal two-terminal mechanical element (referred to as a mechanical one-port). The two terminals (A and B) have absolute

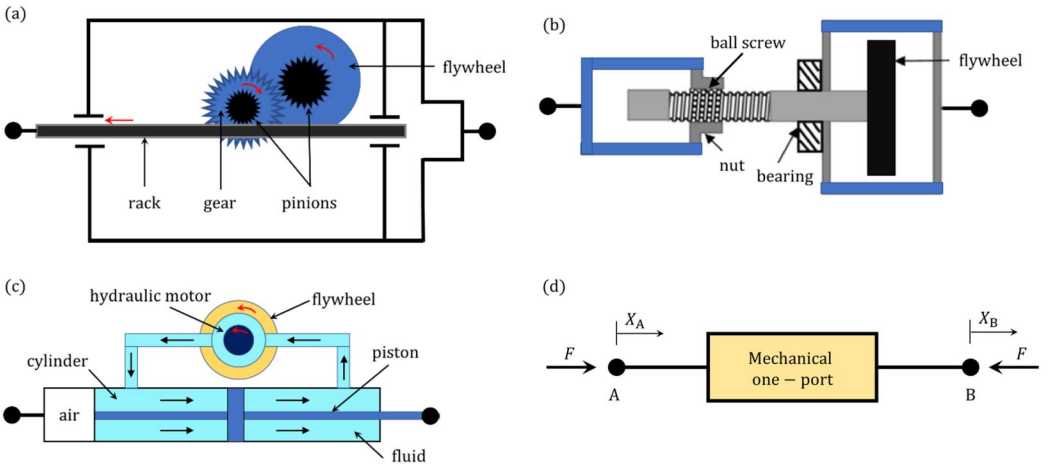

Figure 1. Schematic of (a) rack-and-pinion type inerters, (b) ball-screw type inereters, (c) hydraulic type inerters, and (d) a simplified model of a linear inerter.

displacements X_A and X_B, respectively. A dot over X_A or X_B refers to its time derivative. The forces F at the terminals are equal and opposite, and they are proportional to the relative acceleration between them. Generally, the inertia force generated by the inerter is expressed as $F = b(\ddot{X}_B - \ddot{X}_A)$, in which $b > 0$ is the inertance of the inerter has units of kilograms.

2.2. Analytical models of the TTMDGI-structure systems

In this study, there are three configurations of the TTMDGI are proposed. It should be noted that a TTMD includes two undamped TMDs (TMD1 and TMD2) in parallel, and they are connected together by a bridging dashpot C_{12}. The mass and stiffness of TMD1 are M_1 and K_1, respectively, while the main parameters of TMD2 are the mass M_2 and the stiffness K_2. The main structure has the generalized stiffness (K_s), the mass (M_s) and the damping coefficient (C_s). The external force acting on the structure is assumed as a harmonic force excitation $F(t) = F_0 e^{j\omega t}$ with the excitation frequency ω, the force magnitude F_0 and $j = \sqrt{-1}$.

Three analytical models of the main structure with each TTMDGI configuration are mentioned in this section. The first model is the TTMDGI12-structure system, as shown in Fig. 2, where the TTMDGI12 configuration is a TTMD linked to the ground through two linear inerters (with the inertance values of b_1 and b_2) at TMD1 and TMD2, respectively. The second model is the TTMDGI1-structure system (as described in Fig. 3), in which the TTMDGI1 configuration is based on a TTMD and a grounded inerter at the TMD1 with the corresponding inertance value of b_1. The remaining model is the TTMDGI2-structure system (as presented in Fig. 4), where the TTMDGI2 configuration is a TTMD grounded by an inerter having inertance value of b_2 at the TMD2. From the analytical models of the systems, the free body diagrams of the systems are established and are shown in Figs. 2(b), 3(b), and 4(b). It is assumed that the friction is ignored in all systems and the governing equations of motion of each system are obtained based on the D'Alembert's principle.

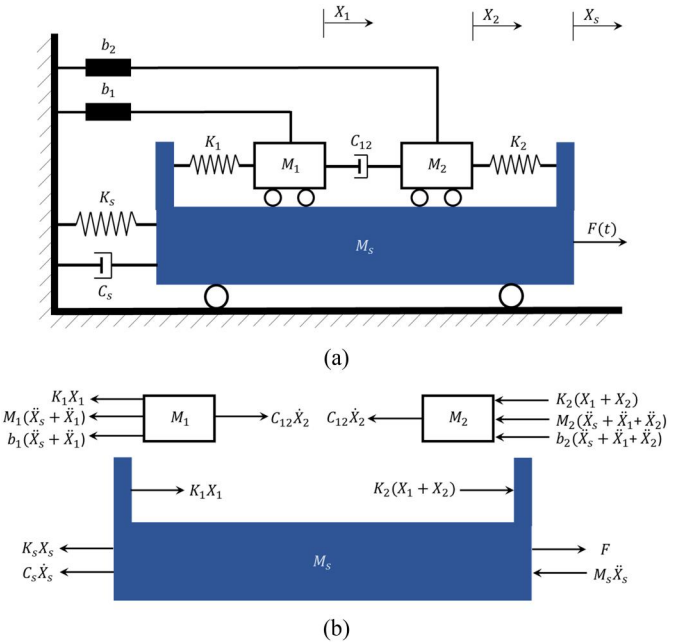

Figure 2. (a) Analytical model of the system with the TTMDGI12 and (b) free body diagrams of the TTMDGI12-structure system.

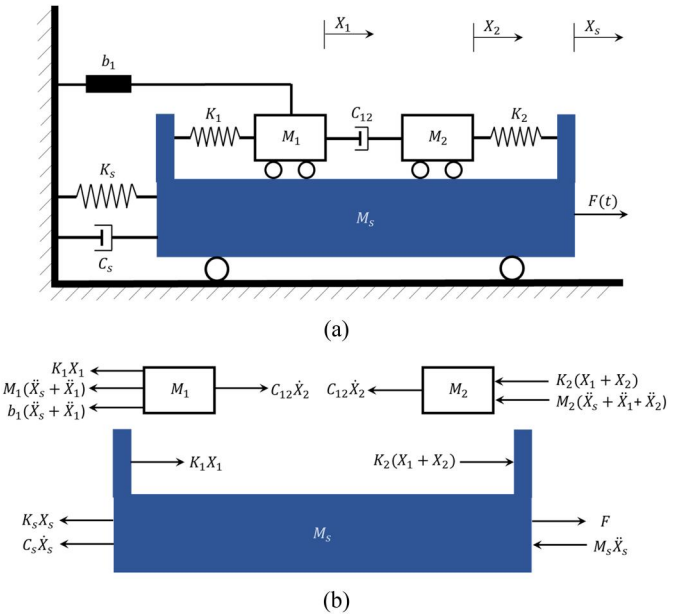

Figure 3. (a) Analytical model of the system with the TTMDGI1 and (b) free body diagrams of the TTMDGI1-structure system.

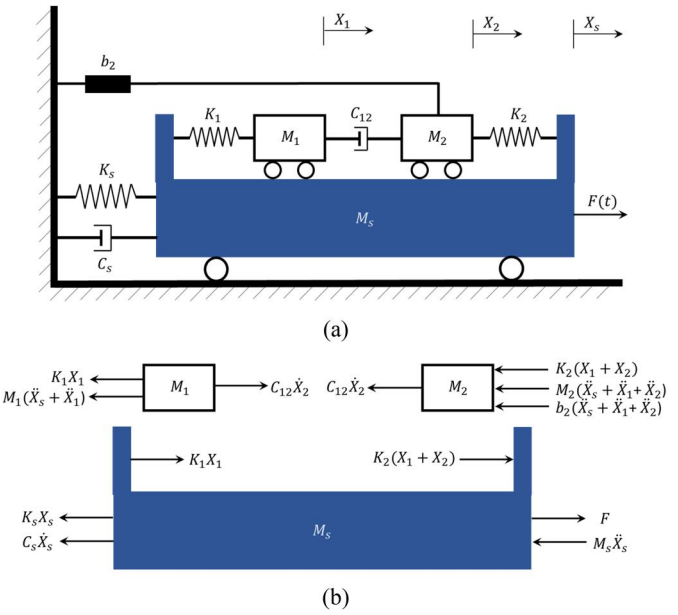

Figure 4. (a) Analytical model of the system with the TTMDGI2 and (b) free body diagrams of the TTMDGI2-structure system.

First, the equations of motion of the main structure equipped with the TTMDGI12 configuration (see Fig. 2) are established. From the free body diagrams of the system are shown in Fig. 2(b), each body is subjected to the external forces and the reactions. Applying D'Alembert's principle, we introduce the inertial forces and add them to the applied forces of each body.

Each body will then be in dynamic equilibrium. In particular, for the body of the main structure, we have

$$M_s\ddot{X}_s(t) + C_s\dot{X}_s(t) + K_sX_s(t) - K_1X_1(t) - K_2(X_1(t) + X_2(t)) - F(t) = 0. \tag{1a}$$

For the body of the TMD1,

$$M_1\left(\ddot{X}_s(t) + \ddot{X}_1(t)\right) + b_1\left(\ddot{X}_s(t) + \ddot{X}_1(t)\right) + K_1X_1(t) - C_{12}\dot{X}_2(t) = 0. \tag{2a}$$

For the body of the TMD2,

$$M_2\left(\ddot{X}_s(t) + \ddot{X}_1(t) + \ddot{X}_2(t)\right) + b_2\left(\ddot{X}_s(t) + \ddot{X}_1(t) + \ddot{X}_2(t)\right) + K_2(X_1(t) + X_2(t)) + C_{12}\dot{X}_2(t) = 0. \tag{3a}$$

From Eqs. (1a), (2a), and (3a), the equations of motion of the TTMDGI12-structure system can be expressed by

$$M_s\ddot{X}_s(t) + C_s\dot{X}_s(t) + K_sX_s(t) - K_1X_1(t) - K_2(X_2(t) + X_1(t)) = F(t), \tag{1b}$$

$$(M_1 + b_1)\ddot{X}_1(t) + K_1X_1(t) - C_{12}\dot{X}_2(t) = -(M_1 + b_1)\ddot{X}_s(t), \tag{2b}$$

$$\left(M_2+b_2\right)\ddot{X}_2(t) + C_{12}\dot{X}_2(t) + K_2(X_2(t) + X_1(t)) = -(M_2 + b_2)\left(\ddot{X}_s(t) + \ddot{X}_1(t)\right). \tag{3b}$$

In the above equations, X_s is the displacement of the main structure, while X_1 is the motion of M_1 relative to the structure, and X_2 is the motion of M_2 relative to M_1. This means that the displacement of the mass M_1 relative to the ground is $X_1^g = X_s + X_1$ and the displacement of the mass M_2 relative to the ground is $X_2^g = X_s + X_1 + X_2$. Importantly, the grounded inerter b_1 generated an inertia force $F_{inerter1} = b_1\ddot{X}_1^g = b_1(\ddot{X}_s + \ddot{X}_1)$ added to the TMD1, and the grounded inerter b_2 generated an inertia force $F_{inerter2} = b_2\ddot{X}_2^g = b_2\left(\ddot{X}_s + \ddot{X}_1 + \ddot{X}_2\right)$ added to the TMD2. Note that a dot over X_i ($i = 1, 2, s$) represents derivation with respect to time t. Now one can write Eqs. (1b), (2b), and (3b) in the matrix form as follows:

$$M\ddot{\mathbf{X}} + C\dot{\mathbf{X}} + KX = F, \tag{4}$$

in which

$$M = \begin{bmatrix} M_s & 0 & 0 \\ M_1 + b_1 & M_1 + b_1 & 0 \\ M_2 + b_2 & M_2 + b_2 & M_2 + b_2 \end{bmatrix}, \tag{4a}$$

$$C = \begin{bmatrix} C_s & 0 & 0 \\ 0 & 0 & -C_{12} \\ 0 & 0 & C_{12} \end{bmatrix}, \tag{4b}$$

$$K = \begin{bmatrix} K_s & -K_1 - K_2 & -K_2 \\ 0 & K_1 & 0 \\ 0 & K_2 & K_2 \end{bmatrix}, \tag{4c}$$

$$F = \begin{bmatrix} F_0 \\ 0 \\ 0 \end{bmatrix} e^{j\omega t}, \tag{4d}$$

$$X = \begin{bmatrix} X_s(t) \\ X_1(t) \\ X_2(t) \end{bmatrix}; \dot{\mathbf{X}} = \begin{bmatrix} \dot{X}_s(t) \\ \dot{X}_1(t) \\ \dot{X}_2(t) \end{bmatrix}; \ddot{\mathbf{X}} = \begin{bmatrix} \ddot{X}_s(t) \\ \ddot{X}_1(t) \\ \ddot{X}_2(t) \end{bmatrix}. \tag{4e}$$

Due to the harmonic force excitation with $F(t) = F_0 e^{j\omega t}$, the responses of the system in the steady state are given by

$$X = \begin{bmatrix} X_s(t) \\ X_1(t) \\ X_2(t) \end{bmatrix} = \begin{bmatrix} \overline{X}_s \\ \overline{X}_1 \\ \overline{X}_2 \end{bmatrix} e^{j\omega t}, \tag{4f}$$

in which $\overline{X}_s$, $\overline{X}_1$ and $\overline{X}_2$ are the peak amplitudes of the structure, mass M_1 and mass M_2. Thus, the vectors $\dot{\mathbf{X}}$ and $\ddot{\mathbf{X}}$ become:

$$\dot{\mathbf{X}} = \begin{bmatrix} \dot{X}_s(t) \\ \dot{X}_1(t) \\ \dot{X}_2(t) \end{bmatrix} = j\omega \begin{bmatrix} \overline{X}_s \\ \overline{X}_1 \\ \overline{X}_2 \end{bmatrix} e^{j\omega t}, \tag{4g}$$

$$\ddot{\mathbf{X}} = \begin{bmatrix} \ddot{X}_s(t) \\ \ddot{X}_1(t) \\ \ddot{X}_2(t) \end{bmatrix} = -\omega^2 \begin{bmatrix} \overline{X}_s \\ \overline{X}_1 \\ \overline{X}_2 \end{bmatrix} e^{j\omega t}. \tag{4h}$$

Substituting Eqs. (4d), (4f)–(4h) into Eq. (4), we have

$$\left(-\omega^2 \mathbf{M} + j\omega \mathbf{C} + \mathbf{K}\right) \begin{bmatrix} \overline{X}_s \\ \overline{X}_1 \\ \overline{X}_2 \end{bmatrix} = \begin{bmatrix} F_0 \\ 0 \\ 0 \end{bmatrix}. \tag{5}$$

Equation (5) is a linear equation. By solving this equation, one can easily determine the maximum amplitude of the structural response in the steady state ($\overline{X}_s$).

The natural frequency of the primary structure

$$\omega_s = \sqrt{\frac{K_s}{M_s}}. \tag{6a}$$

The damping ratio of the primary structure

$$\xi_s = \frac{C_s}{2M_s\omega_s}. \tag{6b}$$

The natural frequency of the TMD1 in the TTMDGI12 is

$$\omega_1 = \sqrt{\frac{K_1}{M_1 + b_1}}. \tag{7}$$

The natural frequency of the TMD2 in the TTMDGI12 is

$$\omega_2 = \sqrt{\frac{K_1}{M_2 + b_2}}. \tag{8}$$

The damping ratio in the TTMDGI12 is

$$\xi_{12} = \frac{C_{12}}{2M_2\omega_2}. \tag{9}$$

The mass ratio of the TMD1 is

$$\mu_1 = \frac{M_1}{M_s} \tag{10a}$$

and the mass ratio of the TMD2 is

$$\mu_2 = \frac{M_2}{M_s}. \tag{10b}$$

Therefore, the actual mass ratio between the TTMDGI12 and the structure is

$$\mu = \frac{M_1 + M_2}{M_s} = \mu_1 + \mu_2 \tag{10c}$$

It is noted that the mass ratio between the TMD2 and the TMD1 in the TTMDGI12 is

$$\mu_{21} = \frac{\mu_2}{\mu_1} = \frac{M_2}{M_1}. \tag{10d}$$

The inertance ratio of the inerter b_1 is defined as

$$\eta_1 = \frac{b_1}{M_s}. \tag{10e}$$

The inertance ratio of the inerter b_2 is defined as

$$\eta_2 = \frac{b_2}{M_s}. \tag{10f}$$

Hence, the total mass ratio between the TTMDGI12 and the structure is determined by

$$\mu^* = \frac{(M_1 + b_1) + (M_2 + b_2)}{M_s} = \mu + \eta_1 + \eta_2, \tag{10g}$$

in which η_1 and η_2 are apparent masses added to the TTMD due to the grounded inerters. This leads to an increase in the mass of TTMDGI12 by $\eta = \eta_1 + \eta_2$ compared with μ in the original TTMD.

It is important to note that the TTMDGI1 configuration (see Fig. 3) is a special case of the TTMDGI12 configuration with $b_2 = 0$. Based on the equations of motion of the system in the first model, one can obtain equations of motion of the system with the TTMDGI1 configuration by substituting $b_2 = 0$ in Eqs. (1b), (2b), and (3b). Here, the equations of motion of the structure coupled with the TTMDGI1 include:

$$M_s\ddot{X}_s(t) + C_s\dot{X}_s(t) + K_sX_s(t) - K_1X_1(t) - K_2(X_2(t) + X_1(t)) = F(t), \tag{11}$$

$$(M_1 + b_1)\ddot{X}_1(t) + K_1X_1(t) - C_{12}\dot{X}_2(t) = -(M_1 + b_1)\ddot{X}_s(t), \tag{12}$$

$$M_2\ddot{X}_2(t) + C_{12}\dot{X}_2(t) + K_2(X_2(t) + X_1(t)) = M_2\left(\ddot{X}_s(t) + \ddot{X}_1(t)\right. \tag{13}$$

The natural frequency of the TMD1 in the TTMDGI1 is

$$\omega_1 = \sqrt{\frac{K_1}{M_1 + b_1}}. \tag{14}$$

The natural frequency of the TMD2 in the TTMDGI1 is

$$\omega_2 = \sqrt{\frac{K_1}{M_2}}. \tag{15}$$

The total mass ratio between the TTMDGI1 and the structure is

$$\mu^* = \frac{(M_1 + b_1)}{M_s} = \mu + \eta_1, \tag{16}$$

Similarly, the TTMDGI2 configuration (see Fig. 4) is the TTMDGI12 configuration without b_1 (or $b_1 = 0$). By replacing $b_1 = 0$ in Eqs. (1b), (2b), and (3b), the equations of motion of the main structure equipped with the TTMDGI2 configuration are:

$$M_s\ddot{X}_s(t) + C_s\dot{X}_s(t) + K_sX_s(t) - K_1X_1(t) - K_2(X_2(t) + X_1(t)) = F(t), \tag{17}$$

$$M_1\ddot{X}_1(t) + K_1X_1(t) - C_{12}\dot{X}_2(t) = -M_1\ddot{X}_s(t), \tag{18}$$

$$(M_2 + b_2)\ddot{X}_2(t) + C_{12}\dot{X}_2(t) + K_2(X_2(t) + X_1(t)) = (M_2 + b_2)\left(\ddot{X}_s(t) + \ddot{X}_1(t)\right), \tag{19}$$

The natural frequency of the TMD1 in the TTMDGI2 is

$$\omega_1 = \sqrt{\frac{K_1}{M_1}}. \tag{20}$$

The natural frequency of the TMD2 in the TTMDGI2 is

$$\omega_2 = \sqrt{\frac{K_1}{M_2 + b_2}}. \tag{21}$$

The total mass ratio between the TTMDGI2 and the structure is determined by

$$\mu^* = \frac{(M_1 + b_2)}{M_s} = \mu + \eta_2, \tag{22}$$

The dynamic magnification factor (DMF) of the structural response in the steady state is given by (Den Hartog 1985; Gil-Martín et al. 2012)

$$DMF = \frac{\overline{X}_s}{(F_0/K_s)} \tag{23}$$

Here, let us introduce some non-dimensional quantities as follows:
The frequency ratio

$$\alpha = \frac{\omega}{\omega_s}. \tag{24}$$

The tuning ratios of each TTMDGI configuration

$$\beta_1 = \frac{\omega_1}{\omega_s} \ \text{(for TMD1)} \tag{25a}$$

and

$$\beta_2 = \frac{\omega_2}{\omega_s} \ \text{(for TMD2)}. \tag{25b}$$

The peak dynamic magnification factor of the structural response (denoted as $DMF_{\max}$) in the frequency range which corresponds to $[\alpha_{lo}, \alpha_{up}]$ can be written by:

$$DMF_{\max} = \frac{\max\left(\overline{X}_s|_{\omega_{lo}}^{\omega_{up}}\right)}{(F_0/K_s)} = \frac{\max\left(\overline{X}_s|_{\alpha_{lo}}^{\alpha_{up}}\right)}{(F_0/K_s)}, \tag{26}$$

in which ω_{lo} and ω_{up} (or α_{lo} and α_{up}) are the lower and upper limits of the excitation frequencies (or frequency ratios), respectively.

It is clear that the frequency response function of the primary structure depends on $\alpha, \xi_s, \beta_1, \beta_2, \ \xi_{12}, b_1, b_2, \mu$ and μ_{21}, in which ξ_s and α are pre-determined for each controlled structure. Additionally, for the purpose of comparison, the TMDI-structure system is also built and its equations of motion are presented in Appendix A, while TTMD-structure system was detailed in Cao, Tran, and Nguyen (2024).

3. Parametric optimization

3.1. Input parameters

In this study, the Yokohama Marine Tower in Japan, a numerical example in many papers (Fujii et al. 1990; Tamura 1998; Tamura et al. 1995), is employed to evaluate the structural vibration control performance of the proposed TTMDGI absorbers. In Fig. 5, the Yokohama Marine Tower is simplified as an SDOF structure. The tower has the mass $M_s = 157$ tons, the natural frequency $f_s = 0.55$ Hz (corresponding to $\omega_s = 3.45$ rad/s) and the damping ratio of the structure $\xi_s = 0.6\%$. The excitation frequency ratio range is assumed to be between 0.5 and 1.5 ($0.5 \leq \alpha \leq 1.5$) and the external force magnitude is $F_0 = 7.5e^5$ N.

In this study, the mass ratio (μ) are respectively fixed to be 0.02 for all cases considered. For each TTMDGI configuration, inertance ratios considered are η_1 or/and η_2 =1, 2, 3, 4, and 5%, while the lower and upper limits of the parameters that need to be optimized are reported in Table 1. An important notice is that the upper limit of ξ_{12} needs to be <1 for the underdamped condition. Thus, the value range of ξ_{12} is chosen to be $0 < \xi_{12} < 0.9$ in this study. In addition, an upper limit of μ_{21} of 500 is large enough for a smaller mass in a TTMD or TTMDGI configuration (e.g. TMD1 or TMD2) which has a weight down to several kilograms.

3.2. Design optimization

3.2.1. Optimization procedure

The parametric optimization aims to maximize the vibration control capacity of each TTMDGI configuration. In other words, the $DMF_{\max}$ value of the structural response should be minimized as the excitation frequency varies within the range of $[\omega_{\text{lo}}, \omega_{\text{up}}]$. Therefore, the objective function based on the $DMF_{\max}$ value is given by

$$Objective = \text{Min}\left(DMF_{\max} \Big|_{\omega_{lo}}^{\omega_{up}} \right). \tag{27}$$

As previously discussed, Eq. (27) has many variables and constraints. Hence, a potential optimization algorithm is needed to solve this problem. At present, numerous potential algorithms have been employed to find solutions for optimization issues (Gad 2022; Le-Duc, Nguyen, and Nguyen-Xuan 2020; McCall 2005), in which Particle Swarm Optimization and Genetic Algorithm have been also integrated into machine learning methods (Liu et al. 2022, 2023; Liu and Lu 2022; Xia et al. 2023). Among these methods, Balancing Composite Motion Optimization (BCMO) is a population-based optimization technique recently developed by Le-Duc, Nguyen, and Nguyen-Xuan (2020). The BCMO has shown impressive efficiency, reduced complexity, and quick convergence compared to other population-based optimization algorithms. Furthermore, the BCMO proves to be effective for multi-objective or intricate optimization scenarios that involve numerous variables and constraints (Bui, Mac, and Bui 2023; Bui, Tran, and Cao 2023; Cao, Tran, and Bui 2024; Le-Duc, Nguyen, and Nguyen-Xuan 2020; Tran, Bui, and Cao 2024). For this reason, the BCMO is selected to determine the optimal parameters for each absorber in this work.

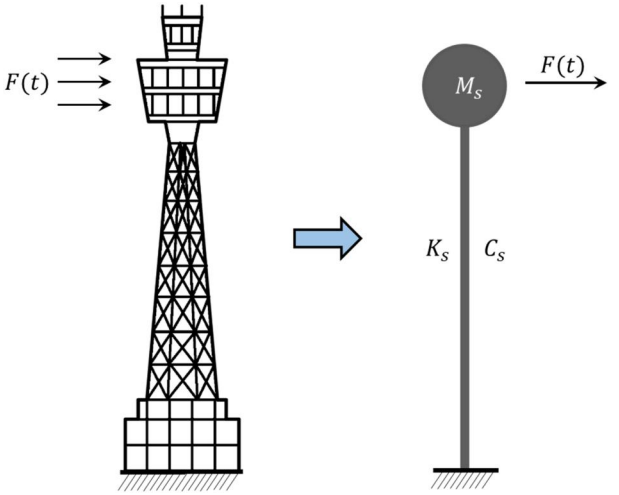

Figure 5. Simplified model of the Yokohama Marine Tower.

Table 1. The lower and upper limits of the parameters of the TTMDGI configurations.

Parameter	Value range	Notation and expression
μ_{21}	$0.05 < \mu_{21} < 500$	$\mu_{21} = \frac{mass\ of\ TMD1}{mass\ of\ TMD2}$
β_1	$0.5 < \beta_1 < 1.5$	The tuning ratio of TMD1
β_2	$0.5 < \beta_2 < 1.5$	The tuning ratio of TMD2
ξ_{12}	$0 < \xi_{12} < 0.9$	The damping ratio of the dashpot

The BCMO algorithm consists of two key parameters: the population size (N_P) and the total number of generations (N_G). These parameters are chosen based on the number of variables in the objective function and its convergence characteristics. A detailed explanation of the BCMO algorithm can be found in Le-Duc, Nguyen, and Nguyen-Xuan (2020), where the authors have made the MATLAB source codes publicly accessible. Figure 6 illustrates the optimization process utilizing the BCMO methodology.

3.2.2. Optimal parameters

Using the input data mentioned in Section 3.1, Table 2 reports the optimized configurations of the TTMD, TTMDGI1, TTMDGI2, and TTMDGI12 for different inertance ratios. For the TTMDGI12 configuration, η_1 is set to be equal to η_2 in all cases considered. For extensive comparisons, Table 3 provides the optimal TMD and TMDI configurations for η values of 1, 2, 3, 4, and 5%. It is noted that all cases calculated in Tables 2 and 3 are for $\mu = 2\%$. To validate the optimal parameters of the TMD obtained from the BCMO algorithm, we can use the explicit formulas of Den Hartog to compute optimal parameters of TMD applied to SDOF structures (Den Hartog 1985). With $\mu = 2\%$, the optimal damping ratio (ξ_T) of TMD is calculated by $\xi_T = \sqrt{\frac{3\mu}{8(1+\mu)}} = 0.086$, and the optimal frequency ratio (β_T) of TMD is calculated by $\beta_T = \frac{1}{(1+\mu)} = 0.980$. Compared to the data presented in Table 3, the optimal parameters of the TMD with the BCMO algorithm agree well with those of the TMD gained from the explicit formulas of Den Hartog.

The optimal parameters shown in Table 2 provide important information about how different design variables interact with the inertance ratio (η). For the TTMDGI12 configuration, it

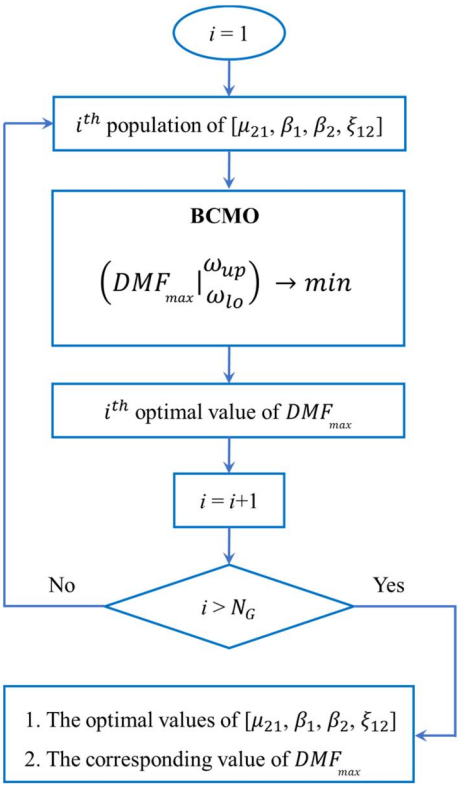

Figure 6. Diagram of the optimization procedure with the BCMO algorithm.

Table 2. Optimal parameters of the TTMDGI configurations with the various values of η_1 or/and η_2.

	Fixed parameters			Optimal parameters			
Configuration or device	η_1	η_2	μ	μ_{21}	β_1	β_2	ξ_{12}
TTMD	0%	0%	2%	0.797	0.888	1.107	0.077
TTMDGI12	1%	1%	2%	1.903	1.153	0.837	0.153
	2%	2%	2%	3.761	1.182	0.805	0.203
	3%	3%	2%	16.185	1.208	0.775	0.250
	4%	4%	2%	498.92	1.207	0.754	0.283
	5%	5%	2%	500.00	1.204	0.740	0.314
TTMDGI1	1%	N/A	2%	5.859	1.132	0.861	0.096
	2%	N/A	2%	5.133	0.839	1.153	0.114
	3%	N/A	2%	499.99	0.825	1.175	0.129
	4%	N/A	2%	500.000	0.806	1.307	0.217
	5%	N/A	2%	500.000	0.785	1.429	0.303
TTMDGI2	N/A	1%	2%	0.539	1.132	0.859	0.154
	N/A	2%	2%	0.194	1.153	0.839	0.300
	N/A	3%	2%	0.050	1.207	0.824	0.773
	N/A	4%	2%	0.086	1.356	0.814	0.900
	N/A	5%	2%	0.138	1.500	0.810	0.900

suggests that as the inertance ratio rises, two design variables including μ_{21} and ξ_{12} also increase. However, this is not totally true for the TTMDGI1 and TTMDGI2 configurations. Among the three inerter-based vibration absorbers in Table 2, the value of ξ_{12} always increases when the inertance ratio rises. Moreover, one can see from Table 2 that when η_1 of the TTMDGI1 configuration increases by or larger than 4%, the optimal μ_{21} value of TTMDGI1 reaches its upper limit (μ_{21}=500). Similarly, the optimal ξ_{12} value of TTMDGI2 also reaches its upper limit (ξ_{12}=0.9)

Table 3. Optimal parameters of the TMDI with the different values of η.

	Fixed parameters		Optimal parameters	
Configuration/device	η	μ	β_T	ξ_T
TMD	N/A	2%	0.979	0.086
TMDI	1%	2%	0.969	0.129
	2%	2%	0.960	0.169
	3%	2%	0.951	0.214
	4%	2%	0.941	0.259
	5%	2%	0.933	0.293

when η_1 of this configuration is equal to or larger than 4%. Obviously, these are disadvantages of the TTMDGI1 and TTMDGI2 configurations compared to the TTMDGI12 configuration. These results emphasize the complexity of the design process and the necessity of considering multiple interrelated factors when optimizing the inerter-based configurations of TTMD.

Meanwhile, the data presented in Table 3 indicates that the value of ξ_T rises while the tuning ratio β_T consistently declines as η increases from 1 to 5%. It is noted that the analytical model and equations of motion of the TMDI-structure are presented in Appendix A.

On the other hand, the computational time of the BCMO algorithm needs for each simulation case is also provided here. With a CPU configuration of Core i7-1185G7, the RAM of 16 GB, and simulation cases performed on MATLAB R2020a software, the computational time for each simulation case of the TTMD or TTMDGI (corresponding to the BCMO parameters of N_P=400, N_G =300) is about 61 s, while the computational time required for each simulation case of the TMD or TMDI with N_P=200 and N_G=150 is about 33 s.

4. Results and discussions

The control performance of each TTMDGI configuration in reducing structural vibrations is mentioned here. Moreover, the effects of the inertance ratio on the structure response and the robustness of TTMDGI configurations are also discussed in this section.

4.1. Effectiveness of TTMDGI configurations

To assess the vibration absorption ability of each TTMDGI configuration, the control performance of each optimized TTMDGI configuration is computed and compared with that of the optimal TMD, TMDI, and TTMD, which have the same weight or/and inertance value as the TTMDGI.

4.1.1. Evaluation criteria

In this work, the vibration control capability of TTMDGI configurations are evaluated based on the $DMF_{\max}$ value (Gao, Kwok, and Samali 1999; Yamaguchi and Harnpornchai 1993) and the root mean square (RMS) of the peak displacement response (RMS_X) (Wu et al. 2018; Xue et al. 2016). For both these criteria, a damper with a smaller $DMF_{\max}$ (or RMS_X) value is more effective (Gao, Kwok, and Samali 1999; Wu et al. 2018; Xue et al. 2016; Yamaguchi and Harnpornchai 1993). In the following equations, the subscripts "US" and "device" are for the uncontrolled system and the system with a device, respectively. Here, the vibration reduction based on the $DMF_{\max}$ value (denoted as R_{DMF}) can be expressed as

$$R_{DMF} = \frac{DMF_{\max,US} - DMF_{\max,device}}{DMF_{\max,US}} \times 100\%. \tag{28}$$

The value of RMS_X in the frequency range corresponding to $[\omega_{lo}, \omega_{up}]$ is given by (Cao 2023, 2025)

$$RMS_X = \sqrt{\frac{\sum_1^n \left(\frac{\overline{X}_{si}}{F_0/K_s}\right)^2}{n}}, \tag{29}$$

in which $\overline{X}_{si}$ represents the sampling value of the structural peak displacement at the excitation frequency ω_i in the frequency range of $[\omega_{lo}, \omega_{up}]$ and the structural stiffness $K_s = M_s\omega_s^2$. It is noted that the RMS_X value calculated in the above equation is a dimensionless quantity. Thus, the vibrating energy reduction based on RMS_X for an absorber is defined by

$$R_{RMS} = \frac{RMS_{X,US} - RMS_{X,device}}{RMS_{X,US}} \times 100\%, \tag{30}$$

4.1.2. Vibration control effectiveness

Based on the data shown in Table 2 (for TTMD and TTMDGI configurations) and Table 3 (for TMD and TMDI), the values of $DMF_{\max}$, R_{DMF}, RMS_X, and R_{RMS} of each damper are determined. These values for the TTMD and TTMDGI configurations at $\mu = 2\%$ are listed in Table 4, while Table 5 provides the $DMF_{\max}$, R_{DMF}, RMS_X, and R_{RMS} values of the optimal TMD and TMDI with $\mu = 2\%$ for the purpose of comparation. For the uncontrolled case, the values of $DMF_{\max}$ and RMS_X of the structure are 83.333 and 11.384, respectively.

As previously discussed, a damper that provides a lower $DMF_{\max}$ value is more effective. This is also true when applied to the RMS_X value. From the evaluation criteria reported in Table 4 regarding the optimal inerter-based configurations of TTMD, one can observe that the performance of TTMD is significantly enhanced when adding one or two grounded inerters to the TTMD. For the TTMDGI12 configuration, this performance improvement rises from 2.4 to 4.7% and from 5.4 to 12.8% for the R_{RMF} and R_{DMF} indicators, respectively, when the inertance ratio increases from 1 to 5%. Meanwhile, this performance improvement of the TTMDGI1 or the TTMDGI2 is lower than that of the TTMDGI12. Furthermore, for the inerter-based configurations of TTMD, the device with a larger inertance ratio is more effective. In this aspect, we can replace the linear inerters in the TTMDGI configurations with improved inerters from the research work by Pirrotta, Di Nardo, and Masnata (2024) to amplify the inertance ratio. This can further improve the vibration control capacity of the TTMDGI configurations.

Table 4. Values of $DMF_{\max}$, R_{DMF}, RMS_X, and R_{RMS} of the TTMD, TTMDGI1, TTMDGI2, and TTMDGI12 configurations.

	Fixed parameters			Evaluation criteria			
Configuration or device	η_1	η_2	μ	$DMF_{\max}$	R_{DMF}	RMS_X	R_{RMS}
TTMD	N/A	N/A	2%	7.257	91.3%	4.070	64.2%
TTMDGI12	1%	1%	2%	5.296	93.6%	3.454	69.7%
	2%	2%	2%	4.398	94.7%	3.123	72.6%
	3%	3%	2%	3.864	95.4%	2.906	74.5%
	4%	4%	2%	3.531	95.8%	2.738	76.0%
	5%	5%	2%	3.359	96.0%	2.607	77.1%
TTMDGI1	1%	N/A	2%	6.033	92.8%	3.700	67.5%
	2%	N/A	2%	5.291	93.7%	3.453	69.7%
	3%	N/A	2%	4.806	94.2%	3.270	71.3%
	4%	N/A	2%	4.757	94.3%	3.153	72.3%
	5%	N/A	2%	4.560	94.5%	3.060	73.1%
TTMDGI2	N/A	1%	2%	6.033	92.8%	3.701	67.5%
	N/A	2%	2%	5.290	93.7%	3.452	69.7%
	N/A	3%	2%	4.943	94.1%	3.275	71.2%
	N/A	4%	2%	4.860	94.2%	3.164	72.2%
	N/A	5%	2%	4.670	94.4%	3.064	73.1%

Table 5. Values of $DMF_{\max}$, R_{DMF}, RMS_X, and R_{RMS} of the TMD and TMDI with $\mu = 2\%$.

		Evaluation criteria			
Configuration or device	Inertance ratio (η)	$DMF_{\max}$	R_{DMF}	RMS_X	R_{RMS}
TMD	N/A	9.104	89.1%	4.367	61.6%
TMDI	1%	7.587	90.9%	4.367	61.6%
	2%	6.661	92.0%	3.703	67.5%
	3%	6.017	92.8%	3.511	69.2%
	4%	5.539	93.4%	3.358	70.5%
	5%	5.163	93.8%	3.222	71.7%

On the other hand, with the same weight and inertance ratio, optimized TTMDGI1, TTMDGI2, and TTMDGI12 configurations are more effective than an optimal TMDI. At $\mu =$ 2%, the $DMF_{\max}$ value reduces from 9.5 to 20.6% when using the optimal TTMDGI1 or TTMDGI2 instead of the TMDI, while this value decreases from 30.2 to 36.3% when using the optimal TTMDGI12 instead of TMDI. Moreover, the RMS_X value of the system with the optimal TTMDGI1 (or TTMDGI2) and TTMDGI12 also reduces from 4.9 to 15.3% and from 15.7 to 20.9% compared to the structure equipped with the TMDI, respectively. It can be seen that, to balance reducing mass and maintaining the damping efficiency of TTMDGI configurations, one can design a TTMDGI with a small mass ratio and a large inheritance ratio.

An extensive comparison based on the DMF curves of the structure equipped with different devices: the optimal TMD, TMDI, TTMD, TTMDGI1, TTMDGI2, and TTMDGI12 at μ=2% is illustrated in Fig. 7, where the inerter-based devices are designed with an inertance ratio of 2%. The figure clearly shows that the peak dynamic magnification factor of the structural response is significantly reduced when employing the optimal inerter-based vibration absorbers. Furthermore, the data from Fig. 7 demonstrates that three inerter-based configurations of TTMD offer superior control performance across a wider excitation frequency range compared to the TMDI, in which the TTMDGI12 configuration is the best. In particular, the TTMDGI1 and TTMDGI2 configurations yield the same $DMF_{\max}$ value of 5.29, while the TTMDGI12 configuration achieves a $DMF_{\max}$ value of 4.40 which is much lower than the $DMF_{\max}$ value of 6.66 obtained with the TMDI configuration. It is important to emphasize that the outstanding advantage of an inerter-based device is the mass amplification effect, which enables it to achieve an apparent mass much greater than its actual physical mass.

To make the discussion clearer, let us look at Figs. 8(a)–8(d) which present DMF response surfaces of the primary structure controlled by the inerter-based devices (including TTMDGI12, TTMDGI1, TTMDGI2, and TMDI configurations) as the inertance ratios change from 1 to 5%. It should be noted that these four absorbers are designed for a mass ratio of 2%. One can observe from Figs. 8(a) and 8(d) that the DMF surface of the system with the TTMDGI12 displays a three-peak characteristic (see Fig. 8a), whereas the response surface of the structure with the TMDI shows a two-peak characteristic (see Fig. 8d) across the inertance ratio range of [1, 5%].

Meanwhile, the DMF response surfaces of the structure with the TTMDGI1 (see Fig. 8b) and with the TTMDGI2 (see Fig. 8c) are similar, and they present a transformation from a three-peak characteristic (at low inertance ratio) to a two-peak characteristic (at higher inertance ratio). As discussed in the previous section and based on their optimal parameters in Table 2, this can be explained by the fact that when η_1 of the TTMDGI1 configuration increases to 4%, the optimal μ_{21} value of TTMDGI1 reaches its upper limit (μ_{21}=500). This means that the mass of TMD2 is very small, and its contribution to vibration reduction is insignificant. In other words, the TTMDGI1 configuration becomes a one-mass damper. For the TTMDGI2 configuration, when the value of η_2 is equal to or larger than 4%, the optimal ξ_{12} value also reaches its upper limit ($\xi_{12} = 0.9$). With a high damping ratio $\xi_{12} = 0.9$, the system approaches the critical damping condition. It is evident that, with a configuration that requires a larger inertance ratio (e.g. η_1 or $\eta_2 > 0.5$), the TTMDGI1 and TTMDGI2 configurations reveal disadvantages.

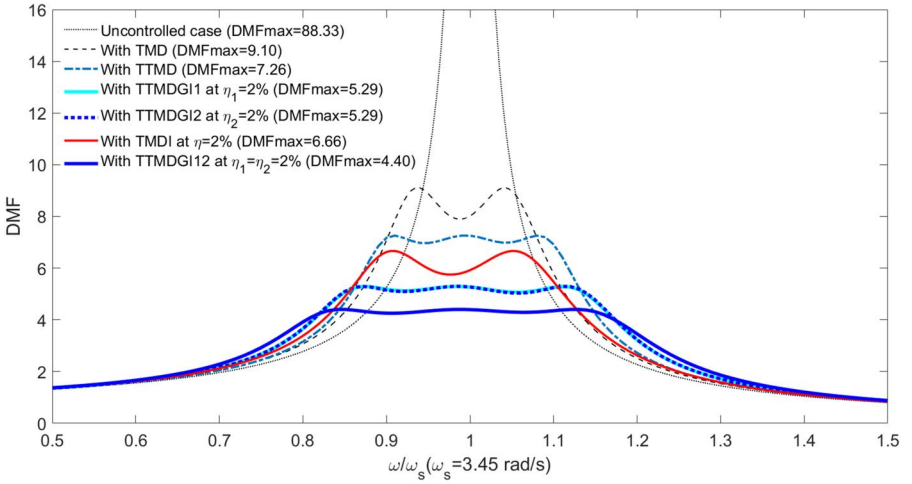

Figure 7. Frequency response functions of the structure with each absorber at $\mu = 2\%$.

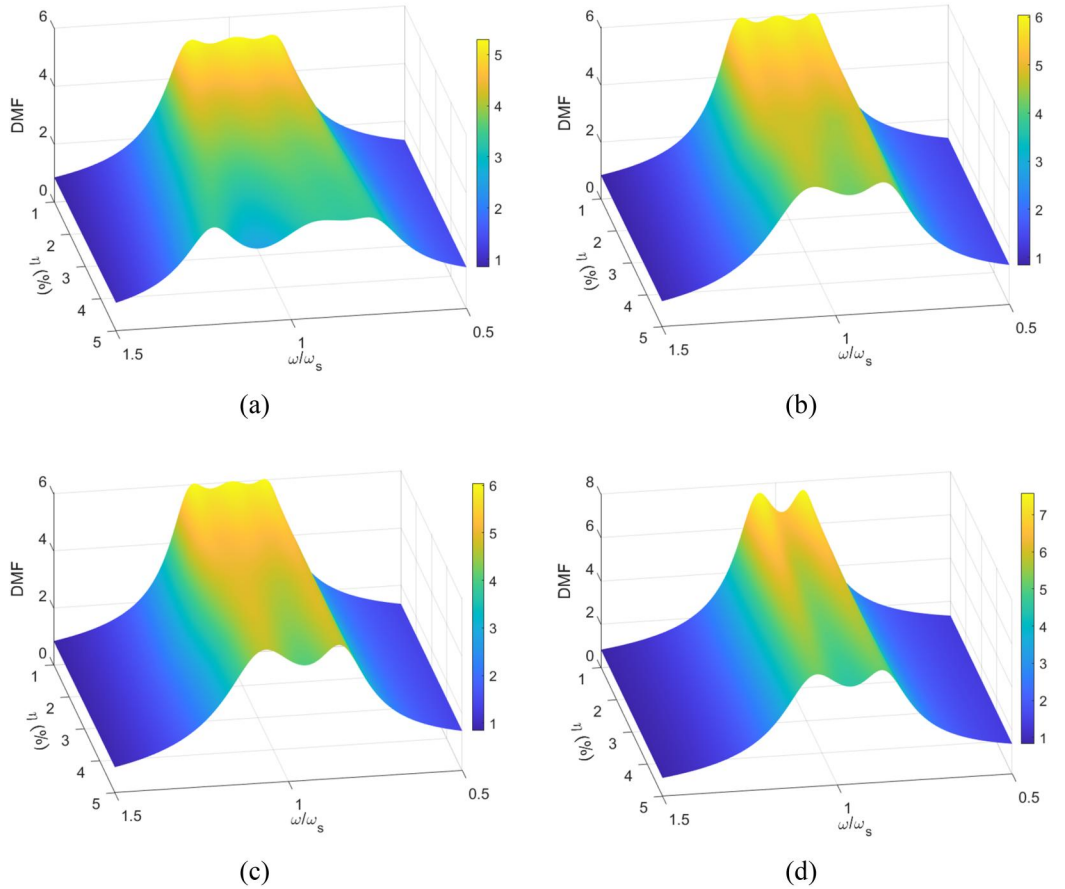

Figure 8. DMF surfaces of the structure controlled by (a) TTMDGI12, (b) TTMDGI1, (c) TTMDGI2, and (d) TMDI at $\mu = 2\%$ when the inertance ratio changes from 1 to 5%.

An important point is that the control performance of the TTMDGI12 is always higher than those of the TTMDGI1 and TTMDGI2. This can be explained by the fact that the total mass ratio of the TTMDGI12 to the primary structure is larger those of TTMDGI1 and TTMDGI2 configurations. In particular, the total mass ratio of the TTMDGI12 is determined by $\mu + \eta_1 + \eta_2$, as expressed in Eq. (10g), while the total mass ratio of TTMDGI1 and TTMDGI2 configurations to the main structure are $\mu + \eta_1$ (see Eq. (16)) and $\mu + \eta_2$ (see Eq. (22)), respectively.

4.2. Effects of the inertance ratio and mass ratio on the structural response

The control performance of three proposed configurations (TTMDGI1, TTMDGI2, and TTMDGI12) directly depends on the inertance and mass ratios. Thus, the effects of the inertance ratio and the mass ratio on the structural vibration reduction will be discussed here. In this investigation, considering the variation of the inertance and mass ratios in the same range of [1, 5%], Figs. 9(a)–9(d) show the $DMF_{\max}$ response surfaces of the structure controlled by the TTMDGI12, TTMDGI1, TTMDGI2 and TMDI configurations, respectively. It is observed that the TTMDGI12 configuration offers the lowest $DMF_{\max}$ surface of the structural response, while this surface of the TTMDGI1 is similar to that of the TTMDGI2 one. The TMDI configuration has the highest $DMF_{\max}$ surface among the four configurations. In other words, the TTMDGI12, TTMDGI1, and TTMDGI2 configurations yield higher control performance compared to the TMDI configuration if considering the same weight and the inertance ratio, in which the TTMDGI12 is the best configuration among three upgraded configurations of TTMD. This means

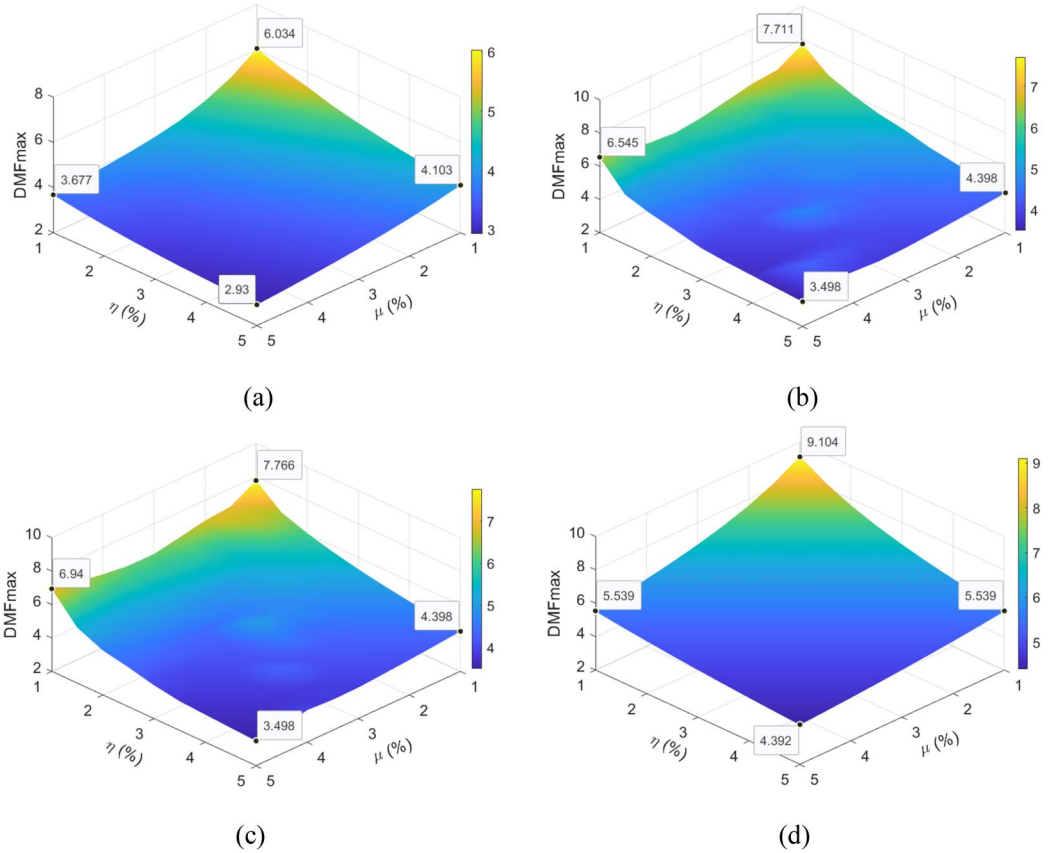

Figure 9. Effects of the inertance ratio and mass ratio on the response of the main structure controlled by (a) the TTMDGI12 configuration, (b) the TTMDGI1 configuration, (c) the TTMDGI2 configuration, and (d) the TMDI as μ and η change from 1 to 5%.

that there is a significant reduction in the device's weight added to the primary structure if one of the TTMDGI12, TTMDGI1, and TTMDGI2 configurations is used instead of TMDI. From the results obtained in Fig. 9, the maximum reduction in the device's weight added to the primary structure is about 4% of the structural mass if using any optimal configurations of TTMDGI12, TTMDGI1, or TTMDGI2 rather than an optimal TMDI configuration. For example, an optimal TTMDGI12 with $\eta_1 = \eta_2 = 5\%$ and $\mu = 1\%$ (with $DMF_{\max} = 4.103$) is more effective than an optimized TMDI with $\eta = \mu = 5\%$ (with $DMF_{\max} = 4.392$). Or an optimal TTMDGI1 or TTMDGI2 configuration with $\eta_1 = \eta_2 = 5\%$ and $\mu = 1\%$ ($DMF_{\max} = 4.398$) is as effective as an optimized TMDI with $\eta = \mu = 5\%$ ($DMF_{\max} = 4.392$).

As shown in Fig. 9(a), the $DMF_{\max}$ value of the structure equipped with a TTMDGI12 configuration optimized drops from 6.034 (corresponding to the optimal TTMDGI12 configuration with $\eta_1 = \eta_2 = \mu = 1\%$) to 2.93 (with the same configuration at $\eta_1 = \eta_2 = \mu = 5\%$). For the optimized TMDI configurations, the $DMF_{\max}$ value of the system reduces from 9.104 (with the TMDI configuration at $\eta = \mu = 1\%$) to 4.392 (for the optimized TMDI configuration with $\eta = \mu = 5\%$) (see Fig. 9d). It is evident that an optimal TTMDGI12 configuration yields significantly higher effectiveness compared to a TMDI. Meanwhile, the TTMDGI1 and TTMDGI2 offer similar control performance when they are designed with the same mass and inertance ratios (see Figs. 9b and 9c). For example, the effectiveness of the optimal TTMDGI1 configuration at $\mu = \eta_1 = 1\%$ is comparable to that of the optimal TTMDGI2 configuration at $\mu = \eta_2 = 1\%$ (7.711 compared to 7.766).

In another aspect, the $DMF_{\max}$ surfaces embody the Pareto optimization surfaces for TTMDGI12, TTMDGI1, TTMDGI2, and TMDI. These surfaces address three core objectives: the weight of the device added to the primary structure, the inertance ratio needed from the grounded inerter, and the performance of vibration reduction. This provides engineers with a framework to balance design goals concerning mass, inertance, and the efficiency of each absorber implemented.

4.3. Effects of changes in structural frequency on the effectiveness of TTMDGI

The natural frequency of the primary structure depends on the stiffness K_s and mass M_s, and it may change due to several reasons. For example, it may come from equipment replacement on the structure, environmental impacts, such as snow accumulation (Xue et al. 2016), or errors in measurement work (Yamaguchi and Harnpornchai 1993). In other words, the natural frequency ω_s of the structure may differ from the initial calculated values. In such cases, the proposed TTMDGI configurations are detuned (Cao 2023). Hence, a study of the robustness of the TTMDGI for changes in the structural frequency will be mentioned in this section.

The variation of the natural frequency compared to the initial calculated value, denoted as $\Delta\omega_s(\%)$, is assumed in the range of [−10, 10%]. Figure 10 shows the robustness of the optimal TMD, TMDI, TTMD, TTMDGI1, TTMDGI2 and TTMDGI12 as $\Delta\omega_s$ varies from −10 to 10%. All cases considered are at the mass ratios of 2%. The inerter-based dampers are designed for inertance ratios of 2%. As observed from the figure, the robustness of TTMDGI1 and TTMDGI2 is identical, while the optimal TTMDGI12 configuration is the most robust one among the devices mentioned. Three upgraded configurations of TTMD (including TTMDGI1, TTMDGI2, and TTMDGI12) are more significantly robust than the conventional TTMD. Additionally, these configurations also have higher robustness compared to the TMD. It can be concluded that the three inerter-based configurations of TTMD are much more robust than the TTMD, and the TTMDGI12 configuration is more robust than the TMDI with the same weight and inertance (especially as the structural frequency decreases).

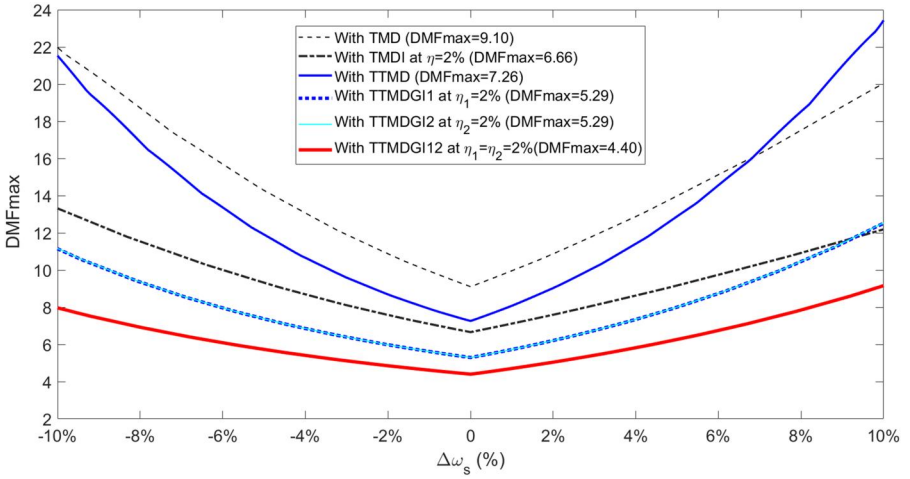

Figure 10. Effect of changes in the structural natural frequency on the effectiveness of the optimal TMD, TMDI, TTMD, and TTMDGI at $\mu = 2\%$.

5. Conclusions

Three configurations of TTMDGI utilized for vibration control of civil structures were proposed in this work. Three corresponding analytical models of the system with one of these TTMDGI configurations were established. After that, the optimal parameters of each TTMDGI configuration for different values of inertance were found using the BCMO algorithm. The effectiveness and robustness of each TTMDGI configuration were investigated. Moreover, the effects of the mass and inertance of each TTMDGI configuration on its control performance were also discussed. The noteworthy findings are drawn from this study as follows:

- Three inerter-based configurations of TTMD are much more effective and robust than the optimal TTMD, in which the TTMDGI12 is the best among vibration absorbers considered. The TTMDGI1 configuration is as effective and robust as the TTMDGI2 configuration.
- At the mass ratio of 2% and with the same inertance, each optimal TTMDGI configuration yields higher performance over a wider excitation frequency range compared to the optimal TMDI. The $DMF_{\max}$ value reduces from 9.5 to 20.6% when using the optimal TTMDGI1 or TTMDGI2, and from 30.2 to 36.3% when using the TTMDGI12 compared to using the TMDI. Furthermore, the RMS_X value of the system with the optimal TTMDGI1 (or TTMDGI2) and TTMDGI12 also decreases from 4.9 to 15.3% and from 15.7 to 20.9% compared to that of the structure equipped with the TMDI, respectively.
- Using a TTMDGI configuration instead of a TMDI also offers a significant reduction in the additional weight of the device on the primary structure. The maximum reduction in the device's weight added to the main structure is about 4% of the structural mass if using any optimal configurations of TTMDGI12, TTMDGI1, or TTMDGI2 rather than an optimal TMDI with the same inertance ratio.
- The TTMDGI12 configuration is more robust than the TMDI with the same mass and inertance ratios (especially as the structural frequency decreases).
- The optimal configuration of TTMDGI with a higher inertance ratio requires a greater damping ratio of the dashpot (ξ_{12}). This is also a disadvantage for the TTMDGI2 configuration.

In practice applications, the models presented in this paper are feasible for large-scale structures. However, connecting the inerter directly to the ground can be challenging for tall civil

structures, such as high-rise buildings or towers. In such cases, rigid support columns or tensioned cables can be employed, as mentioned in the literature (Xiang, Nishitani, and Wu 2017; Xiang and Nishitani 2017). One can use a mechanical transmission system (e.g. cable-pulley system, rigid rods, or hydraulic/pneumatic lines) to bridge the distance between the absorber and the anchor point on the ground. In addition, the TTMDI configurations are more complex than the TMDI because the number of components in a TTMDI configuration is larger than that of a TMDI. This also results in an increase in the maintenance cost compared to using a TMDI.

While the findings in this work are based on the harmonic excitation force, these inerter-based configurations of TTMD are also expected to be effective under random excitations. Although the frequency response curve of the TTMDGI-structure system is relatively flat over a wider frequency range compared to the TMD (Fig. 7), the TTMDGI configurations are tuned to the specific frequency of vibration. Similar to TMDs, they may be less effective against vibrations if there are changes in their damping, stiffness, and inertance coefficients compared to their optimal values. In the future, the sensitivity to changes in the damping, stiffness, and inertance coefficients of the TTMDGI configuration will be investigated, and we will also expand this study to demonstrate the effectiveness of the TTMDGI configurations in suppressing the vibration of MDOF structures subjected to wind and earthquake loads. The next research direction of the paper is to apply Physics-Informed Neural Networks (PINNs) (Cuomo et al. 2022; Liu et al. 2024) to calculate the optimal parameters of TTMDGI. PINNs offer several advantages, including the ability to directly optimize the TTMDGI parameters during the training process, which eliminates the need for traditional optimization loops. This leads to a significant reduction in computation time, especially for complex systems. Moreover, PINNs are well-suited for modeling multi-degree-of-freedom (MDOF) systems, especially when TTMDGI is attached to large or nonlinear structures. Additionally, PINNs can be easily extended to different structural systems or under various dynamic conditions, such as wind or earthquakes.

Disclosure statement

No potential conflict of interest was reported by the author(s).

Funding

This research was supported by Vietnam Maritime University.

ORCID

Quoc-Huong Cao http://orcid.org/0000-0002-6352-3787

Data availability statement

All data that support the findings of this study are included within the article.

References

Baduidana, M., and A. Kenfack-Jiotsa. 2024. "Parameters Optimization of Three-Element Dynamic Vibration Absorber with Inerter and Grounded Stiffness." *Journal of Vibration and Control* 30 (7–8): 1548–1565. https://doi.org/10.1177/10775463231164698

Balendra, T., C. M. Wang, and H. F. Cheong. 1995. "Effectiveness of Tuned Liquid Column Dampers for Vibration Control of Towers." *Engineering Structures* 17 (9): 668–675. https://doi.org/10.1016/0141-0296(95)00036-7

Bui, H.-L., N.-A. Tran, and H. Q. Cao. 2023. "Active Control Based on Hedge-Algebras Theory of Seismic-Excited Buildings with Upgraded Tuned Liquid Column Damper." *Journal of Engineering Mechanics* 149 (1): 04022091. https://doi.org/10.1061/JENMDT.EMENG-6821

Bui, V.-B., T.-T. Mac, and H.-L. Bui. 2023. "Design Optimization considering the Stability Constraint of the Hedge-Algebras-Based Controller for Building Structures Subjected to Seismic Excitations." Proceedings of the Institution of Mechanical Engineers, Part I: Journal of Systems and Control Engineering, 09596518231171960.

Cao, H. Q. 2023. "Combined Tuned Mass Dampers for Structural Vibration Control." *International Journal of Non-Linear Mechanics* 157: 104550. https://doi.org/10.1016/j.ijnonlinmec.2023.104550

Cao, H. Q. 2025. "A Comparative Study on the Effectiveness, Robustness and Mistuning Sensitivity of Upgraded Tuned Mass Dampers in Mitigating the Dynamic Response of Civil Structures." *Archive of Applied Mechanics* 95 (3) Article 71. https://doi.org/10.1007/s00419-025-02781-z

Cao, H. Q., and N.-A. Tran. 2023. "Multi-Objective Optimal Design of Double Tuned Mass Dampers for Structural Vibration Control." *Archive of Applied Mechanics* 93 (5): 2129–2144. https://doi.org/10.1007/s00419-023-02376-6

Cao, H. Q., N.-A. Tran, and H.-L. Bui. 2024. "Hedge-Algebras-Based Hybrid Control of Earthquake-Induced Buildings Using Upgraded Tuned Liquid Column Dampers." *Soil Dynamics and Earthquake Engineering* 182: 108728. https://doi.org/10.1016/j.soildyn.2024.108728

Cao, H. Q., N.-A. Tran, and X.-T. Nguyen. 2024. "Tuned Two-Mass Dampers for Vibration Control of Offshore Platforms." *Engineering Research Express* 6 (3): 35511.

Cao, Q. H. 2021. "Vibration Control of Structures by an Upgraded Tuned Liquid Column Damper." *Journal of Engineering Mechanics* 147 (9): 04021052. https://doi.org/10.1061/(ASCE)EM.1943-7889.0001965

Chillemi, M., T. Furtmüller, C. Adam, and A. Pirrotta. 2023. "Nonlinear Mechanical Model of a Fluid Inerter." *Mechanical Systems and Signal Processing* 188: 109986. https://doi.org/10.1016/j.ymssp.2022.109986

Cuomo, S., V. S. Di Cola, F. Giampaolo, G. Rozza, M. Raissi, and F. Piccialli. 2022. "Scientific Machine Learning Through Physics–Informed Neural Networks: Where We Are and What's Next." *Journal of Scientific Computing* 92 (3): 88. https://doi.org/10.1007/s10915-022-01939-z

Den Hartog, J. P. 1985. *Mechanical Vibrations*. New York, NY: Dover Publications, Inc.

Fujii, K., Y. Tamura, T. Sato, and T. Wakahara. 1990. "Wind-Induced Vibration of Tower and Practical Applications of Tuned Sloshing Damper." *Journal of Wind Engineering and Industrial Aerodynamics* 33 (1–2): 263–272. https://doi.org/10.1016/0167-6105(90)90042-B

Gad, A. G. 2022. "Particle Swarm Optimization Algorithm and Its Applications: A Systematic Review." *Archives of Computational Methods in Engineering* 29 (5): 2531–2561. https://doi.org/10.1007/s11831-021-09694-4

Gao, H., K. S. C. Kwok, and B. Samali. 1999. "Characteristics of Multiple Tuned Liquid Column Dampers in Suppressing Structural Vibration." *Engineering Structures* 21 (4): 316–331. https://doi.org/10.1016/S0141-0296(97)00183-1

Giaralis, A., and F. Petrini. 2017. "Wind-Induced Vibration Mitigation in Tall Buildings Using the Tuned Mass-Damper-Inerter." *Journal of Structural Engineering* 143 (9): 04017127.

Gil-Martín, L. M., J. F. Carbonell-Márquez, E. Hernández-Montes, M. Aschheim, and M. Pasadas-Fernández. 2012. "Dynamic Magnification Factors of SDOF Oscillators under Harmonic Loading." *Applied Mathematics Letters* 25 (1): 38–42. https://doi.org/10.1016/j.aml.2011.07.005

Kendo-Nouja, B., M. Baduidana, A. Kenfack-Jiotsa, and R. Nzengwa. 2024. "Vibration Reduction of Primary Structure Using Optimum Grounded Inerter-Based Dynamic Vibration Absorber." *Archive of Applied Mechanics* 94 (1): 137–156. https://doi.org/10.1007/s00419-023-02513-1

Konar, T., and A. Ghosh. 2024. "Tuned Mass Damper Inerter for Seismic Control of Multi-Story Buildings: Ten Years since Inception." *Structures* 63: 106459. https://doi.org/10.1016/j.istruc.2024.106459

Le-Duc, T., Q.-H. Nguyen, and H. Nguyen-Xuan. 2020. "Balancing Composite Motion Optimization." *Information Sciences* 520: 250–270. https://doi.org/10.1016/j.ins.2020.02.013

Liu, B., and W. Lu. 2022. "Surrogate Models in Machine Learning for Computational Stochastic Multi-Scale Modelling in Composite Materials Design." *International Journal of Hydromechatronics* 5 (4): 336–365. https://doi.org/10.1504/IJHM.2022.127037

Liu, B., N. Vu-Bac, X. Zhuang, W. Lu, X. Fu, and T. Rabczuk. 2023. "Al-DeMat: A Web-Based Expert System Platform for Computationally Expensive Models in Materials Design." *Advances in Engineering Software* 176: 103398. https://doi.org/10.1016/j.advengsoft.2022.103398

Liu, B., N. Vu-Bac, X. Zhuang, X. Fu, and T. Rabczuk. 2022. "Stochastic Full-Range Multiscale Modeling of Thermal Conductivity of Polymeric Carbon Nanotubes Composites: A Machine Learning Approach." *Composite Structures* 289: 115393. https://doi.org/10.1016/j.compstruct.2022.115393

Liu, B., Y. Wang, T. Rabczuk, T. Olofsson, and W. Lu. 2024. "Multi-Scale Modeling in Thermal Conductivity of Polyurethane Incorporated with Phase Change Materials Using Physics-Informed Neural Networks." *Renewable Energy*. 220: 119565. https://doi.org/10.1016/j.renene.2023.119565

Liu, X., J. Z. Jiang, B. Titurus, and A. Harrison. 2018. "Model Identification Methodology for Fluid-Based Inerters." *Mechanical Systems and Signal Processing* 106: 479–494. https://doi.org/10.1016/j.ymssp.2018.01.018

Ma, R., K. Bi, and H. Hao. 2021. "Inerter-Based Structural Vibration Control: A State-of-the-Art Review." *Engineering Structures* 243: 112655. https://doi.org/10.1016/j.engstruct.2021.112655

Madhamshetty, K., and J. M. Manimala. 2018. "Low-Rate Characterization of a Mechanical Inerter." *Machines* 6 (3): 32. https://doi.org/10.3390/machines6030032

Marian, L., and A. Giaralis. 2014. "Optimal Design of a Novel Tuned Mass-Damper–Inerter (TMDI) Passive Vibration Control Configuration for Stochastically Support-Excited Structural Systems." *Probabilistic Engineering Mechanics* 38: 156–164. https://doi.org/10.1016/j.probengmech.2014.03.007

Masnata, C., A. Di Matteo, C. Adam, and A. Pirrotta. 2023. "Nontraditional Configuration of Tuned Liquid Column Damper Inerter for Base-Isolated Structures." *Mechanics Research Communications* 129: 104101. https://doi.org/10.1016/j.mechrescom.2023.104101

McCall, J. 2005. "Genetic Algorithms for Modelling and Optimisation." *Journal of Computational and Applied Mathematics* 184 (1): 205–222. https://doi.org/10.1016/j.cam.2004.07.034

Momtaz, A. A., M. A. Abdollahian, and A. Farshidianfar. 2017. "Study of Wind-Induced Vibrations in Tall Buildings with Tuned Mass Dampers Taking into account Vortices Effects." *International Journal of Advanced Structural Engineering* 9 (4): 385–395. https://doi.org/10.1007/s40091-017-0174-9

Pandey, D. K., and S. K. Mishra. 2021. "Inerter Assisted Robustness of Compliant Liquid Column Damper." *Structural Control and Health Monitoring* 28 (8), p.n/a. https://doi.org/10.1002/stc.2763

Pietrosanti, D., M. De Angelis, and A. Giaralis. 2020. "Experimental Study and Numerical Modeling of Nonlinear Dynamic Response of SDOF System Equipped with Tuned Mass Damper Inerter (TMDI) Tested on Shaking Table under Harmonic Excitation." *International Journal of Mechanical Sciences* 184: 105762. https://doi.org/10.1016/j.ijmecsci.2020.105762

Pietrosanti, D., M. De Angelis, and M. Basili. 2020. "A Generalized 2-DOF Model for Optimal Design of MDOF Structures Controlled by Tuned Mass Damper Inerter (TMDI)." *International Journal of Mechanical Sciences* 185: 105849. https://doi.org/10.1016/j.ijmecsci.2020.105849

Pirrotta, A., L. A. Di Nardo, and C. Masnata. 2024. "Theoretical and Experimental Investigation on an Improved Rack and Pinion Inerter." *Nonlinear Dynamics* 2024-10. https://doi.org/10.1007/s11071-024-10532-y

Shah, M. U., and M. Usman. 2022. "An Experimental Study of Tuned Liquid Column Damper Controlled Multi-Degree of Freedom Structure Subject to Harmonic and Seismic Excitations." *PLOS One* 17 (6): e0269910. https://doi.org/10.1371/journal.pone.0269910

Shen, Y., L. Chen, X. Yang, D. Shi, and J. Yang. 2016. "Improved Design of Dynamic Vibration Absorber by Using the Inerter and Its Application in Vehicle Suspension." *Journal of Sound and Vibration* 361: 148–158. https://doi.org/10.1016/j.jsv.2015.06.045

Smith, M. C. 2002. "Synthesis of Mechanical Networks: The Inerter." *IEEE Transactions on Automatic Control* 47 (10): 1648–1662. https://doi.org/10.1109/TAC.2002.803532

Smith, M. C. 2020. "The Inerter: A Retrospective." *Annual Review of Control, Robotics, and Autonomous Systems* 3 (1): 361–391. https://doi.org/10.1146/annurev-control-053018-023917

Tamura, Y. 1998. "Application of Damping Devices to Suppress Wind-Induced Responses of Buildings." *Journal of Wind Engineering and Industrial Aerodynamics* 74–76: 49–72. https://doi.org/10.1016/S0167-6105(98)00006-3

Tamura, Y., K. Fujii, T. Ohtsuki, T. Wakahara, and R. Kohsaka. 1995. "Effectiveness of Tuned Liquid Dampers under Wind Excitation." *Engineering Structures* 17 (9): 609–621. https://doi.org/10.1016/0141-0296(95)00031-2

Tran, N.-A., H.-L. Bui, and Q.-H. Cao. 2024. "U-Shaped and V-Shaped Tuned Liquid Column Dampers in Vibration Reduction of Earthquake-Induced Buildings: A Comparative Study." *Structures* 65: 106669. https://doi.org/10.1016/j.istruc.2024.106669

Tran, N.-A., V.-B. Hoang, H.-L. Bui, and H. Quoc Cao. 2025. "Upgraded Double Tuned Mass Dampers for Vibration Control of Structures under Earthquakes." *Computers & Structures* 310: 107700. https://doi.org/10.1016/j.compstruc.2025.107700

Wang, Q., N. D. Tiwari, H. Qiao, and Q. Wang. 2020. "Inerter-Based Tuned Liquid Column Damper for Seismic Vibration Control of a Single-Degree-of-Freedom Structure." *International Journal of Mechanical Sciences* 184: 105840. https://doi.org/10.1016/j.ijmecsci.2020.105840

Wu, Q., W. Zhao, W. Zhu, R. Zheng, and X. Zhao. 2018. "A Tuned Mass Damper with Nonlinear Magnetic Force for Vibration Suppression with Wide Frequency Range of Offshore Platform under Earthquake Loads." *Shock and Vibration* 2018: 1–18.

Xia, Y., C. Zhang, C. Wang, H. Liu, X. Sang, R. Liu, P. Zhao, et al. 2023. "Prediction of Bending Strength of Glass Fiber Reinforced Methacrylate-Based Pipeline UV-CIPP Rehabilitation Materials Based on Machine Learning." *Tunnelling and Underground Space Technology* 140: 105319. https://doi.org/10.1016/j.tust.2023.105319

Xiang, P., A. Nishitani, and M. Wu. 2017. "Seismic Vibration and Damage Control of High-Rise Structures with the Implementation of a Pendulum-Type Nontraditional Tuned Mass Damper." *Structural Control and Health Monitoring* 24 (12), p.n/a. https://doi.org/10.1002/stc.2022

Xiang, P., and A. Nishitani. 2017. "Structural Vibration Control with the Implementation of a Pendulum-Type Nontraditional Tuned Mass Damper System." *Journal of Vibration and Control* 23 (19): 3128–3146. https://doi.org/10.1177/1077546315626821

Xue, Q., J. Zhang, J. He, and C. Zhang. 2016. "Control Performance and Robustness of Pounding Tuned Mass Damper for Vibration Reduction in SDOF Structure." *Shock and Vibration* 2016: 1–15.

Yamaguchi, H., and N. Harnpornchai. 1993. "Fundamental Characteristics of Multiple Tuned Mass Dampers for Suppressing Harmonically Forced Oscillations." *Earthquake Engineering & Structural Dynamics* 22 (1): 51–62. https://doi.org/10.1002/eqe.4290220105

Appendix A.

The TMDI-structure system

An analytical model of the system TMDI-structure under an external force excitation is shown in Fig. A1. The TMD has the mass M_{T} and the stiffness K_{T} and the damping coefficient C_{T}. The equations of motion of the system are expressed by:

$$(M_T + b)\ddot{X}_s(t) + (M_T + b)\ddot{X}_T(t) + C_T\dot{X}_T(t) + K_T X_T(t) = 0, \tag{A1}$$

$$M_s\ddot{X}_s(t) + C_s\dot{X}_s(t) + K_s X_s(t) - C_T\dot{X}_T(t) - K_T X_T(t) = F(t), \tag{A2}$$

in which X_s is the structural displacement relative to the ground and X_{T} is the displacement of the TMD relative to the structure.

The natural frequency of the TMDI is

$$\omega_{\mathrm{T}} = \sqrt{\frac{K_{\mathrm{T}}}{M_{\mathrm{T}} + b}} \tag{A3}$$

The damping ratio of the TMD is

$$\xi_{\mathrm{T}} = \frac{C_{\mathrm{T}}}{2M_{\mathrm{T}}\omega_{\mathrm{T}}} \tag{A4}$$

The mass ratio between the TMD and structure is

$$\mu_{\mathrm{T}} = \frac{M_{\mathrm{T}}}{M_s} \tag{A5}$$

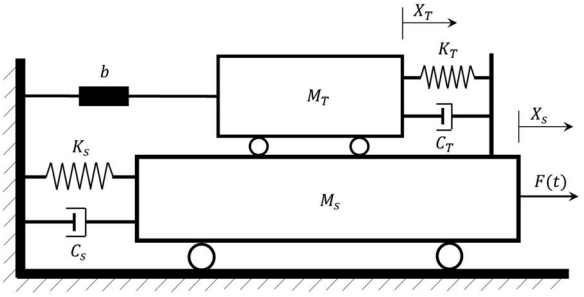

Figure A1. Analytical model of the TMDI-structure system.

The total mass ratio between the TMDI and the structure is given by

$$\overline{\mu} = \mu_{\mathrm{T}} + \eta, \tag{A6}$$

in which η is the inertance ratio of the inerter.

The tuning ratio of the TMDI is

$$\beta_{\mathrm{T}} = \frac{\omega_{\mathrm{T}}}{\omega_s}. \tag{A7}$$